Article

Cell Reports

Synaptic Targeting and Function of SAPAPs Mediated by Phosphorylation-Dependent Binding to PSD-95 MAGUKs

Graphical Abstract

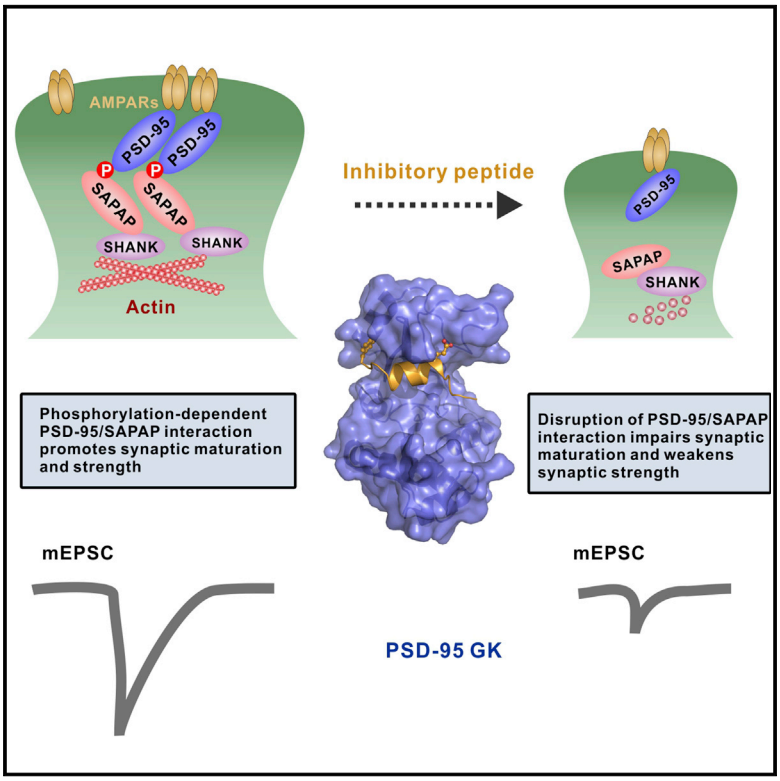

Highlights

- Phosphorylation-dependent complex formation revealed by the SAPAP/PSD-95 structure
- Phosphorylation is required for synaptic targeting and maturation functions of SAPAPs
- A potent non-phosphorylated PSD-95 GK inhibitory peptide is developed
- This PSD-95 inhibitory peptide weakens excitatory synaptic strength

Authors

Jinwei Zhu, Qingqing Zhou, Yuan Shang, ..., Guoping Feng, Youming Lu, Mingjie Zhang

Correspondence

mzhang@ust.hk

In Brief

Using structural biology, cell biology, and electrophysiology approaches, Zhu et al. demonstrate that phosphorylation of the N-terminal repeating sequences of SAPAPs is required for the SAPAP/PSD-95 complex formation and SAPAP's synaptic targeting and maturation functions. They also developed a potent non-phosphorylated PSD-95 GK inhibitory peptide that can effectively disrupt the SAPAP/PSD-95 complex formation and thus inhibit excitatory synaptic activities.

Data and Software Availability

5YPO
5YPR

Zhu et al., 2017, Cell Reports *21*, 3781–3793
December 26, 2017
https://doi.org/10.1016/j.celrep.2017.11.107

CellPress

Cell Reports
Article

Synaptic Targeting and Function of SAPAPs Mediated by Phosphorylation-Dependent Binding to PSD-95 MAGUKs

Jinwei Zhu,[1,2,3,12] Qingqing Zhou,[3,12] Yuan Shang,[3] Hao Li,[4,5] Mengjuan Peng,[1,2,6] Xiao Ke,[4,5] Zhuangfeng Weng,[1,2,6] Rongguang Zhang,[1,2,6] Xuhui Huang,[7,11] Shawn S.C. Li,[8] Guoping Feng,[9,10] Youming Lu,[4,5] and Mingjie Zhang[3,11,13,*]
[1]National Center for Protein Science Shanghai, CAS Center for Excellence in Molecular Cell Science, Shanghai Institute of Biochemistry and Cell Biology, Chinese Academy of Sciences, Shanghai 201203, China
[2]University of Chinese Academy of Sciences, 333 Haike Road, Shanghai 201203, China
[3]Division of Life Science, State Key Laboratory of Molecular Neuroscience, Hong Kong University of Science and Technology, Clear Water Bay, Kowloon, Hong Kong, China
[4]Department of Physiology, School of Basic Medicine and Tongji Medical College, Huazhong University of Science and Technology, Wuhan 4030030, China
[5]The Institute for Brain Research, Collaborative Innovation Center for Brain Science, Huazhong University of Science and Technology, Wuhan 430030, China
[6]School of Life Science and Technology, ShanghaiTech University, 100 Haike Road, Shanghai 201210, China
[7]Department of Chemistry, Hong Kong University of Science and Technology, Clear Water Bay, Kowloon, Hong Kong, China
[8]Department of Biochemistry, Siebens-Drake Medical Research Institute, Schulich School of Medicine and Dentistry, University of Western Ontario, London, ON N6A 5C1, Canada
[9]McGovern Institute for Brain Research, Department of Brain and Cognitive Sciences, Massachusetts Institute of Technology, Cambridge, MA 02139, USA
[10]Stanley Center for Psychiatric Research, Broad Institute of MIT and Harvard, Cambridge, MA 02142, USA
[11]Center of Systems Biology and Human Health, Hong Kong University of Science and Technology, Clear Water Bay, Kowloon, Hong Kong, China
[12]These authors contributed equally
[13]Lead Contact
*Correspondence: mzhang@ust.hk
https://doi.org/10.1016/j.celrep.2017.11.107

SUMMARY

The PSD-95/SAPAP/Shank complex functions as the major scaffold in orchestrating the formation and plasticity of the post-synaptic densities (PSDs). We previously demonstrated that the exquisitely specific SAPAP/Shank interaction is critical for Shank synaptic targeting and Shank-mediated synaptogenesis. Here, we show that the PSD-95/SAPAP interaction, SAPAP synaptic targeting, and SAPAP-mediated synaptogenesis require phosphorylation of the N-terminal repeat sequences of SAPAPs. The atomic structure of the PSD-95 guanylate kinase (GK) in complex with a phosphor-SAPAP repeat peptide, together with biochemical studies, reveals the molecular mechanism underlying the phosphorylation-dependent PSD-95/SAPAP interaction, and it also provides an explanation of a PSD-95 mutation found in patients with intellectual disabilities. Guided by the structural data, we developed potent non-phosphorylated GK inhibitory peptides capable of blocking the PSD-95/SAPAP interaction and interfering with PSD-95/SAPAP-mediated synaptic maturation and strength. These peptides are genetically encodable for investigating the functions of the PSD-95/SAPAP interaction *in vivo*.

INTRODUCTION

Dendritic spines are tiny membrane protrusions from dendritic shafts, and they play critical roles in synaptic transmissions. The post-synaptic density (PSD) at the distal tip of dendritic spine heads refers to a densely packed multi-protein structure orchestrating synaptic formation and function (Carlin et al., 1980; Chen et al., 2008; Sheng and Kim, 2011). As central signal transduction hubs at synapses, the PSDs are enriched with neurotransmitter receptors, adhesion molecules, scaffold proteins, signaling enzymes, and cytoskeletal components (Bayés and Grant, 2009; Dieterich and Kreutz, 2016; Kim and Sheng, 2004; Sheng and Hoogenraad, 2007). Scaffold proteins serve as bridges linking the upstream glutamate receptors (i.e., NMDA-type glutamate receptors [NMDARs] and AMPA-type glutamate receptors [AMPARs]) with the downstream signaling complexes and cytoskeletons. Accordingly, spatial and temporal organization of scaffold protein-mediated protein complexes at the core of the PSD is pivotal for synaptic signaling and plasticity (Won et al., 2017; Zhu et al., 2016b). Mutations of genes encoding the PSD scaffold proteins have been frequently associated with various psychiatric disorders, including autism

spectrum disorder (ASD), obsessive-compulsive disorder (OCD), intellectual disability (ID), and schizophrenia (Balan et al., 2013; Grant, 2012; Lelieveld et al., 2016; Pinto et al., 2010; Ting et al., 2012; Volk et al., 2015).

The PSD-95 family of membrane-associated guanylate kinases (MAGUKs), including PSD-95, PSD-93, SAP102, and SAP97, are the most abundant scaffold proteins in the PSDs. PSD-95 directly binds to SAPAP (also known as DLGAP or GKAP), which in turn binds to the Shank family proteins, forming the PSD-95/SAPAP/Shank core complex of PSD (Kim et al., 1997; Naisbitt et al., 1999; Takeuchi et al., 1997). This core complex is thought to be critical for synaptic development and transmission. Many lines of evidence have indicated that PSD-95 MAGUKs are essential for trafficking and anchoring of synaptic glutamate receptors (Chen et al., 2015; Elias and Nicoll, 2007; Opazo et al., 2012). Loss of PSD-95 MAGUKs led to a reduction in the number of synapses containing glutamate receptors and defects in both AMPAR and NMDAR transmissions (Levy et al., 2015). Likewise, removal of SAPAP or Shank also results in the loss of AMPAR-containing synapses and weaker synaptic transmissions (Hung et al., 2008; Shin et al., 2012).

Recent super-resolution imaging studies have revealed that major synaptic scaffold proteins, such as PSD-95 and SAPAP, form co-clustered nanodomains with glutamate receptors (e.g., AMPAR) in the PSDs (MacGillavry et al., 2013; Nair et al., 2013). Alteration of the level of PSD-95 changes the number and area of AMPAR nanodomains and synaptic transmissions (MacGillavry and Hoogenraad, 2015; Nair et al., 2013). Importantly, the subsynaptic co-clustering of PSD-95/AMPAR alters in response to synaptic activities (Fukata et al., 2013; MacGillavry and Hoogenraad, 2015; Zhu et al., 2016b), though with poorly understood molecular mechanisms.

Given the fundamental roles that the PSD-95/SAPAP/Shank core complex plays in orchestrating the assembly of the PSDs as well as in regulating the dynamic changes of synaptic morphology and plasticity, it is not surprising that mutations of the genes encoding these proteins can cause severe psychiatric disorders and neurodevelopmental diseases (Grant, 2012; Marín, 2012). For example, *DLG4* (encoding PSD-95) knockout mice showed increased repetitive behaviors and abnormal social behaviors reminiscent of ASD and Williams' syndrome (Feyder et al., 2010). Human genetic studies also indicated that *DLG4* is a possible candidate gene for ID and schizophrenia (Balan et al., 2013; Lelieveld et al., 2016; Rauch et al., 2012). Mice with genetic deletion of *Sapap3* or *Sapap2* exhibited increased anxiety-like and aggressive behaviors relevant to OCD and ASD (Jiang-Xie et al., 2014; Welch et al., 2007). Increasing evidence suggests that the *Sapap* family genes are tightly associated with the neuropathology of ASD, OCD, and Tourette's syndrome in humans (Bienvenu et al., 2009; Crane et al., 2011; Pinto et al., 2010; Stewart et al., 2013; Züchner et al., 2009). Mutations of Shank-encoding genes are highly penetrant in causing ASD (Peça et al., 2011; Pinto et al., 2010; Ting et al., 2012).

A better understanding of the molecular basis underlying the PSD-95/SAPAP/Shank complex formation can provide valuable insights into the physiological roles of the complex in synapse formation and function as well as the mechanisms of brain disorders caused by alterations of these genes. Recent biochemical and structural studies have demonstrated the exquisitely specific interaction between Shank and SAPAP (Zeng et al., 2016). However, how the SAPAP/Shank complex is recruited to the PSDs is still rudimentarily understood. SAPAP1 was shown to bind guanylate kinase (GK) domains of PSD-95 and MAGI2, and the interactions have been mapped to several 14-amino acid repeats (referred to as GK-binding repeats [GBRs]) at the N terminus of SAPAP1 (Hirao et al., 1998; Kim et al., 1997; Naisbitt et al., 1997). We and others have demonstrated that the GK domain of MAGUKs functions as a phosphoprotein-binding module (Johnston et al., 2012; Zhu et al., 2011, 2014). Moreover, phosphor-SAPAP1 GBR peptides have been shown to bind to PSD-95 SH3-GK (Zhu et al., 2011), suggesting that the PSD-95/SAPAP interaction may be regulated by phosphorylation. However, the molecular mechanism governing the phosphorylation-dependent PSD-95/SAPAP interaction has not been elucidated.

In this work, we solved the crystal structure of PSD-95 GK in complex with a synthetic phosphor-SAPAP1 GBR peptide (i.e., pSAPAP1-R2). The complex structure not only elucidates the molecular basis underlying the specific and likely synaptic activity-regulated PSD-95/SAPAP interaction but also provides a mechanistic explanation for the etiology of ID caused by a mutation identified in PSD-95. We further demonstrated that the phosphorylation-dependent PSD-95/SAPAP interaction is crucial for SAPAP synaptic targeting and SAPAP-mediated synaptogenesis. We successfully designed several non-phosphorylated GK inhibitory peptides, and we solved the structure of PSD-95 SH3-GK in complex with one of the GK inhibitory peptides. We went on to demonstrate that the most potent GK inhibitory peptide can effectively block the PSD-95/SAPAP interaction and impair synaptogenesis when expressed in cultured neurons.

RESULTS

Crystal Structure of PSD-95 GK in Complex with a Phosphorylated SAPAP1 Peptide

Analysis of the GBR sequences in the SAPAP family of proteins (SAPAP1–4) reveals a highly consensus motif of -R-x-x-S-Y-x-x-A-, where "x" denotes any residue (Figure 1A). We previously demonstrated that two phosphorylated SAPAP1 GBRs bind to PSD-95 SH3-GK in a fluorescence polarization-based assay (Zhu et al., 2011). Here we first confirmed the PSD-95 GK/SAPAP interaction using purified recombinant PSD-95 GK and two synthetic phosphor-SAPAP peptides (i.e., phosphor-SAPAP1-GBR2 [pSAPAP1-R2] and phosphor-SAPAP3-GBR1 [pSAPAP3-R1]). Isothermal titration calorimetry (ITC)-based assays showed that PSD-95 GK binds to pSAPAP1-R2 and pSAPAP3-R1 with K_d values of ~0.08 and 0.07 μM, respectively (Figure 1B). As expected, the unphosphorylated SAPAP peptides (i.e., SAPAP1-R2 and SAPAP3-R1) displayed no detectable binding to PSD-95 GK (Figure 1B). Given that the sequences of GBR motifs in SAPAPs are extremely conserved, it is expected that all of the phosphor-SAPAP-GBRs can bind to PSD-95 GK with high affinity and dephosphorylation of Ser(0) in each GBR would eliminate its binding to PSD-95.

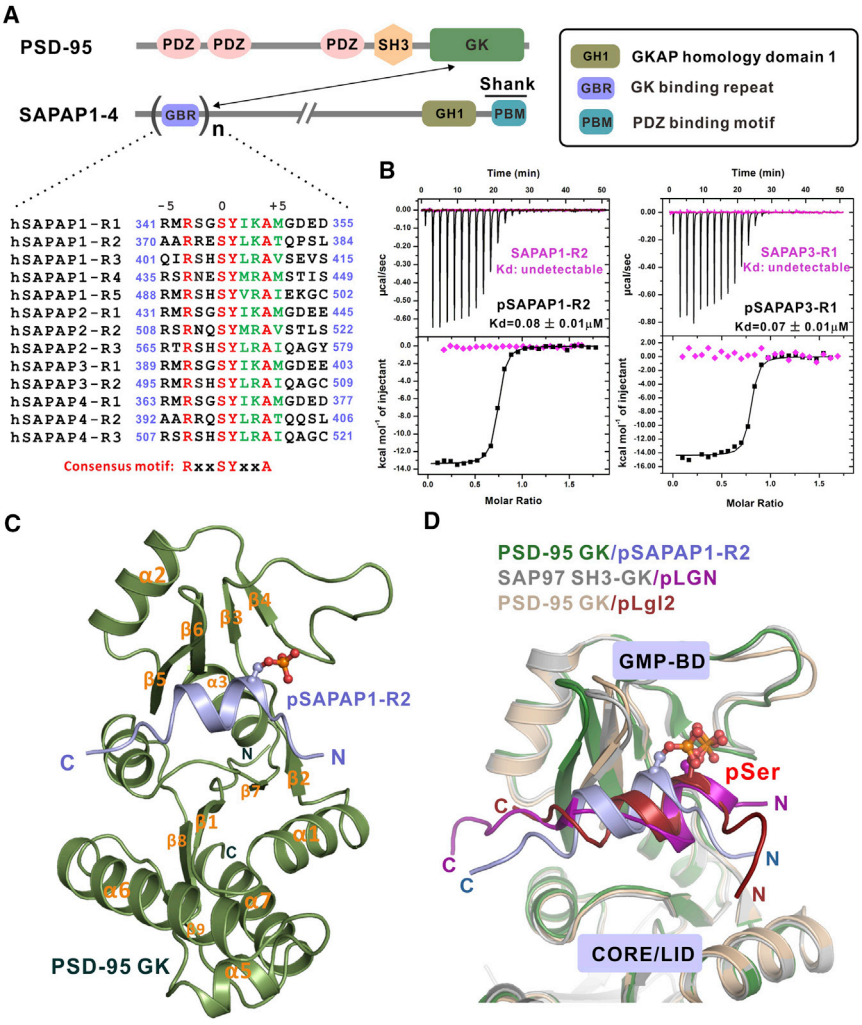

Figure 1. Biochemical and Structural Characterization of PSD-95/SAPAP Interaction

(A) Schematic diagram of the domain organizations of PSD-95 and SAPAP family proteins (SAPAP1–4). The interaction between PSD-95 and SAPAPs is indicated by a two-way arrow. The amino acid sequence alignment of the GK-binding repeat (GBR) of human SAPAPs is also shown. In this alignment, the absolutely conserved and conserved residues are color in red and green, respectively. The consensus GK-binding motif -R-x-x-S-Y-x-x-A- is shown beneath the alignment.

(B) ITC-based measurements of the binding affinities between phosphor- and unphosphor-SAPAP1-R2 or SAPAP3-R1 peptides and PSD-95 GK.

(C) Ribbon diagram representation of the crystal structure of PSD-95 GK in complex with the phosphor-SAPAP1-GBR2 peptide (pSAPAP1-R2). The phosphate group of pSAPAP1-R2 is shown in the ball-and-stick model.

(D) Superposition of the structures of PSD-95 GK/pSAPAP1-R2 (light blue, this study), SAP97 SH3-GK/pLGN (purple; PDB: 3UAT), and PSD-95 GK/pLgl2 (red; PDB: 3WP0).

To better understand the molecular details of the PSD-95 GK/phosphor-SAPAP interaction, we solved the complex structure of PSD-95 GK/pSAPAP1-R2 at 2.3-Å resolution (Table S1). Each asymmetric unit contains two copies of the complex with very similar conformation. In the complex, PSD-95 GK adopts a typical GK domain architecture, and the pSAPAP1-R2 peptide forms a short helix engaging the canonical phosphopeptide-binding pocket of PSD-95 GK (Zhu et al., 2016b) (Figure 1C). Including this study, four crystal structures of DLG GK/phosphopeptide complexes (i.e., SAP97 SH3-GK/pLGN [Zhu et al., 2011], PSD-95 GK/pLgl2 (two structures with distinct pLgl2 peptides) [Zhu et al., 2014], and PSD-95/pSAPAP1-R2 in this study) have been determined. Superposition of these structures reveals several common features of the DLG GK/phosphopeptide interactions (Figure 1D): each bound phosphopeptide contains a short α helix in its N-terminal half; DLG GK recognizes diverse phosphopeptides via similar binding sites formed by the GMP-binding (GMP-BD) and the CORE/LID subdomains; peptide binding does not induce large conformational changes to the DLG GK domains.

The PSD-95 GK/pSAPAP1-R2 Interface

The complex structure reveals that the pSAPAP1-R2-binding site on GK consists of two key elements: the phosphor-site and the hydrophobic site. The phosphate group of the pSAPAP1-R2 is coordinated by side chains of R568, R571, and Y580 at the phosphor-site. These polar interactions are further strengthened by intramolecular interactions between side chains of R568, E574, and Y609 of GK (Figure 2A). As expected, alterations of the phosphor-site of GK (the R568, R571, Y580, and Y609A quadruple mutant) totally disrupted the GK/pSAPAP1-R2 interaction (Figure 2C; Table S2). Substitution of pSer of pSAPAP1-R2 and pSAPAP3-R1 with Ala abolished the GK/pSAPAP1-R2 and GK/pSAPAP3-R1 interactions (Figure 2C). Surprisingly, substitution of pSer of pSAPAP1-R2 and pSAPAP3-R1 with Glu also disrupted the interactions (Figure 2C), suggesting that the Ser-to-Glu substitution in SAPAP GBRs cannot be used as a phosphor-mimetic mutation for investigating the PSD-95/SAPAP interaction. This is distinct from our previous finding that the phosphor-mimetic mutant of LGN could still retain modest binding to DLG GK (Zhu et al., 2011).

The hydrophobic site of GK is occupied by the short α helix formed by pS(0) to T(+5) of pSAPAP1-R2 (Figures 2A and 2B). The side chains of Y(+1) and A(+4) of pSAPAP1-R2 insert into the hydrophobic pocket formed by Y580, Y604, and Y609 from GK (Figure 2B). In addition to forming the hydrophobic interactions with the hydrophobic site of GK, the side chain of Y(+1) of pSAPAP1-R2 forms hydrogen bonds with the side chains of E600 and T611 of GK. This is a unique feature of the GK/pSAPAP

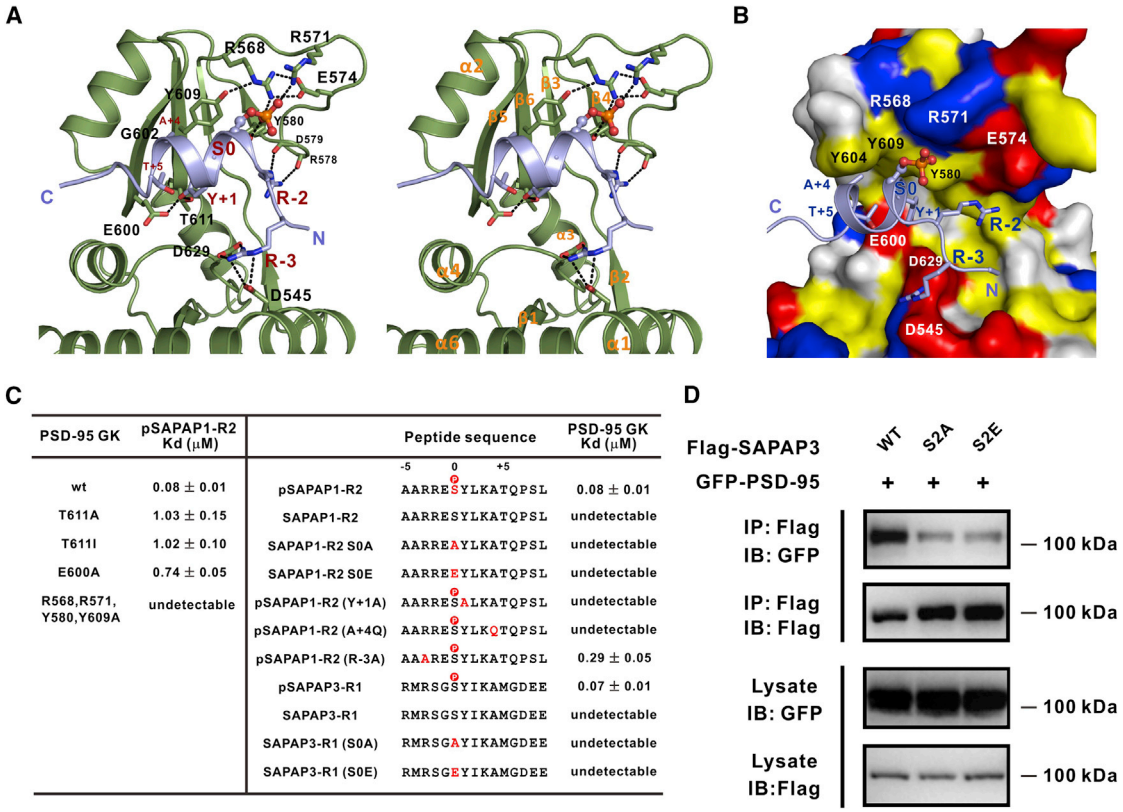

C

PSD-95 GK	pSAPAP1-R2 Kd (μM)
wt	0.08 ± 0.01
T611A	1.03 ± 0.15
T611I	1.02 ± 0.10
E600A	0.74 ± 0.05
R568,R571, Y580,Y609A	undetectable

	Peptide sequence (-5 0 +5)	PSD-95 GK Kd (μM)
pSAPAP1-R2	AARRE(pS)YLKATQPSL	0.08 ± 0.01
SAPAP1-R2	AARRESYLKATQPSL	undetectable
SAPAP1-R2 S0A	AARREAYLKATQPSL	undetectable
SAPAP1-R2 S0E	AARREEYLKATQPSL	undetectable
pSAPAP1-R2 (Y+1A)	AARRE(pS)ALKATQPSL	undetectable
pSAPAP1-R2 (A+4Q)	AARRE(pS)YLKQTQPSL	undetectable
pSAPAP1-R2 (R-3A)	AAARE(pS)YLKATQPSL	0.29 ± 0.05
pSAPAP3-R1	RMRSG(pS)YIKAMGDEE	0.07 ± 0.01
SAPAP3-R1	RMRSGSYIKAMGDEE	undetectable
SAPAP3-R1 (S0A)	RMRSGAYIKAMGDEE	undetectable
SAPAP3-R1 (S0E)	RMRSGEYIKAMGDEE	undetectable

D

Figure 2. Detailed Interface of the PSD-95 GK/pSAPAP1-R2 Complex

(A) Stereo view of detailed interaction between PSD-95 GK and the pSAPAP1-R2 peptide. Dotted lines denote hydrogen bonds and salt bridge interactions.

(B) The combined ribbon and surface representation of the PSD-95 GK/pSAPAP1-R2 complex. The hydrophobic residues, positively charged residues, and negatively charged residues of GK are color in yellow, blue, and red, respectively.

(C) Summary of ITC-based measurements of the binding affinities between the wild-type and mutants of PSD-95 GK and the pSAPAP1-R2 peptide.

(D) CoIP assay showing that both the S394, 500A (S2A) and S394, 500E (S2E) mutants of SAPAP3 significantly decreased their bindings to PSD-95.

interaction compared to other GK/target interactions (Zhu et al., 2011, 2014, 2016a). In line with the critical roles of Y(+1) and A(+4) of pSAPAP1-R2 in the complex formation, substitutions of either Y(+1) with Ala or A(+4) with Gln eliminated the GK/pSAPAP1-R2 interaction (Figure 2C). Importantly, substitution of either T611 or E600 from GK with Ala also significantly weakened its binding to pSAPAP1-R2 (Figure 2C), supporting the specific role of the hydrogen bonds between these two residues and the hydroxyl group of Y(+1) observed in the complex structure (Figure 2A; also see Figure 6 discussing a PSD-95 mutation found in ID patients).

Besides the residues involved in the two major interaction sites discussed above, several polar interactions further contribute to the specific GK/pSAPAP1-R2 interaction. For example, the side chain of R(-3) of pSAPAP1-R2 forms charge-charge interactions with the side chains of D545 and D629 of GK. The side chain of R(-2) of pSAPAP1-R2 forms hydrogen bonds with the main chains of R578 and D579 from GK. Fitting the structural analysis, substitution of R(−3) with Ala weakened the binding of pSAPAP1-R2 to GK by ~3.5-fold (Figure 2C).

We then tested the phosphorylation-dependent interaction between the full-length PSD-95 and the full-length SAPAP expressed in heterologous cells. We used the FLAG-tagged wild-type (WT) SAPAP3 or its mutants for co-immunoprecipitation (coIP) of GFP-tagged PSD-95. SAPAP3 contains two GBR motifs (Figure 1A). We verified that the SAPAP3-R1 peptide binds to PSD-95 GK also in a strict phosphorylation-dependent manner. Substitution of pSer(0) with Ala or Glu also eliminated the binding of pSAPAP3-R1 to PSD-95 (bottom four rows in the right column of Figure 2C). As expected, SAPAP3 WT showed a robust binding to PSD-95 in the coIP assay (Figure 2D). Both the phosphor-deficient mutant (S394, 500A, referred to as S2A) and the phosphor-mimetic mutant (S394, 500E, referred to as S2E) of SAPAP3 showed significantly weaker binding to PSD-95 (Figure 2D). Our data are consistent with a report showing that both the phosphor-deficient mutant (S54, 201A double mutant) and phosphor-mimetic mutant (S54, 201D double mutant) of SAPAP1 displayed diminished bindings to PSD-95 GK in yeast two-hybrid assays (Shin et al., 2012). Taken together, we concluded that phosphorylation of GBR motifs in SAPAP is critical for the PSD-95/SAPAP interaction and the S/E substitutions in the SAPAP GBRs cannot be used to mimic phosphorylation-induced binding of SAPAP to PSD-95.

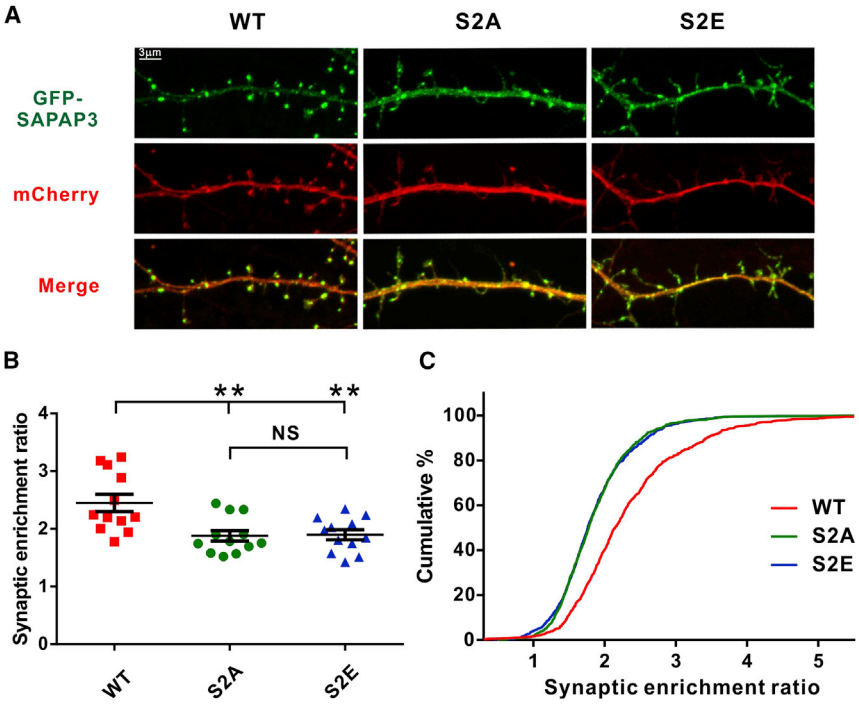

Figure 3. Phosphorylation-Dependent PSD-95/SAPAP Interaction Is Crucial for the Synaptic Targeting of SAPAP

(A) Representative images of transfected hippocampal neurons at DIV17.

(B and C) Quantification of the imaging data showing synaptic targeting of various SAPAP3 constructs. Synaptic enrichment ratio of SAPAP3 is defined as: $[GFP_{spine}/GFP_{shaft}]/[mCherry_{spine}/mCherry_{shaft}]$. Twelve neurons (i.e., n = 12) from four independent batches of cultures were imaged for each group for quantifications. Error bar indicates ± SEM. **p < 0.01; NS, not significant. One-way ANOVA with Tukey's multiple comparison test was used for the plot in (B). (C) shows the cumulative frequency plot of synaptic enrichment ratio of various forms of SAPAP3.

Phosphorylation-Dependent PSD-95/SAPAP Interaction Is Critical for SAPAP Synaptic Targeting and Dendritic Spine Development

Since PSD-95 and SAPAP colocalize with each other along dendritic spines in cultured hippocampal neurons (Kim et al., 1997; Shin et al., 2012), we next investigated whether the phosphorylation-dependent PSD-95/SAPAP interaction is required for the synaptic targeting of SAPAP. The GFP-tagged SAPAP3 WT and its two PSD-95 binding-deficient mutants, S2A and S2E, were individually co-transfected with mCherry in cultured hippocampal neurons at day *in vitro* 14 (DIV14). Neurons were fixed for further imaging analysis at DIV17. As expected, the expressed GFP-SAPAP3 WT showed prominent spine localization, whereas both the S2A and S2E mutants of SAPAP3 were less enriched in spines and more diffused to dendritic shafts (Figure 3A). Quantitative synaptic enrichment ratio data (normalized by mCherry intensity) further confirmed that the synaptic targeting efficiency of the SAPAP3 S2A mutant was significantly lower than SAPAP3 WT (Figures 3B and 3C; WT = 2.45 ± 0.15 and S2A = 1.88 ± 0.09; **p < 0.01, one-way ANOVA with Tukey's multiple comparison test). Notably, SAPAP3 S2E exhibited targeting deficiency very similar to that of SAPAP3 S2A (Figures 3B and 3C; S2E = 1.89 ± 0.09). In line with this observation, in COS-7 cells, the S2D mutant (S54, 201D double mutant) of SAPAP1 did not co-cluster with PSD-95, whereas SAPAP1 WT and PSD-95 formed perfect co-clustering (Kim et al., 1997; Romorini et al., 2004; Shin et al., 2012). Collectively, these data indicate that the phosphorylation-dependent interaction between PSD-95 and SAPAPs is critical for synaptic targeting of SAPAPs.

Dendritic spines undergo dramatic morphological changes during development. In mature neurons, the shapes of spines dynamically change in response to diverse neuronal stimuli, an activity that is tightly associated with various forms of synaptic plasticity. Given that a set of key scaffold proteins (e.g., PSD-95, SAPAP, Shank, Homer, etc.) plays essential roles in synaptic development (Levy et al., 2015; Sala et al., 2001; Zeng et al., 2016), we next evaluated the role of the specific PSD-95/SAPAP interaction in synaptogenesis. In this assay, we classified the spines with a mushroom-like head as mature spines (featuring larger-diameter spine heads), while others, including filopodia-like, stubby, branchy, and thin mushroom, we classified as immature spines. FLAG-tagged SAPAP3 constructs (WT, S2A, and S2E) were transfected into cultured hippocampal neurons (DIV14), and GFP was co-transfected with each SAPAP3 construct to outline the morphology of dendritic spines and as the background transfection control (Figure 4A). Compared to the GFP or SAPAP3 WT group, neurons overexpressing SAPAP S2A or S2E showed more filopodia-like and less mushroom-like spines at DIV17 (Figure 4A). Quantifications of the images revealed that overexpression of either SAPAP3 S2A or SAPAP3 S2E led to a significant reduction in the proportion of mature spines compared to the control neurons (i.e., the GFP-alone group or the SAPAP3 WT group) (Figure 4B; GFP = 0.33 ± 0.02, WT = 0.39 ± 0.03, S2A = 0.15 ± 0.02, and S2E = 0.18 ± 0.02; ***p < 0.001 and ****p < 0.0001, one-way ANOVA with Tukey's multiple comparison test). We also quantified the effect of PSD-95/SAPAP3 interaction on spine morphology by measuring the spine head width using ImageJ software (Zeng et al., 2016). Neurons expressing SAPAP3 WT showed a mild but significant increase of spine head width compared to the control neurons expressing GFP only (Figures 4C and 4D). In contrast, neurons expressing either SAPAP3 S2A or SAPAP3 S2E showed a prominent reduction in spine head width, which is consistent with above mature spine ratio analysis (Figures 4C and 4D; GFP = 0.52 ± 0.01 μm, WT = 0.59 ± 0.03 μm, S2A = 0.41 ± 0.01 μm, and S2E = 0.35 ± 0.01 μm; *p < 0.05, **p < 0.01, ***p < 0.001, and ****p < 0.0001, one-way ANOVA with Tukey's multiple comparison test). The above data indicate that the phosphorylation-dependent interaction between PSD-95 and SAPAP is crucial for

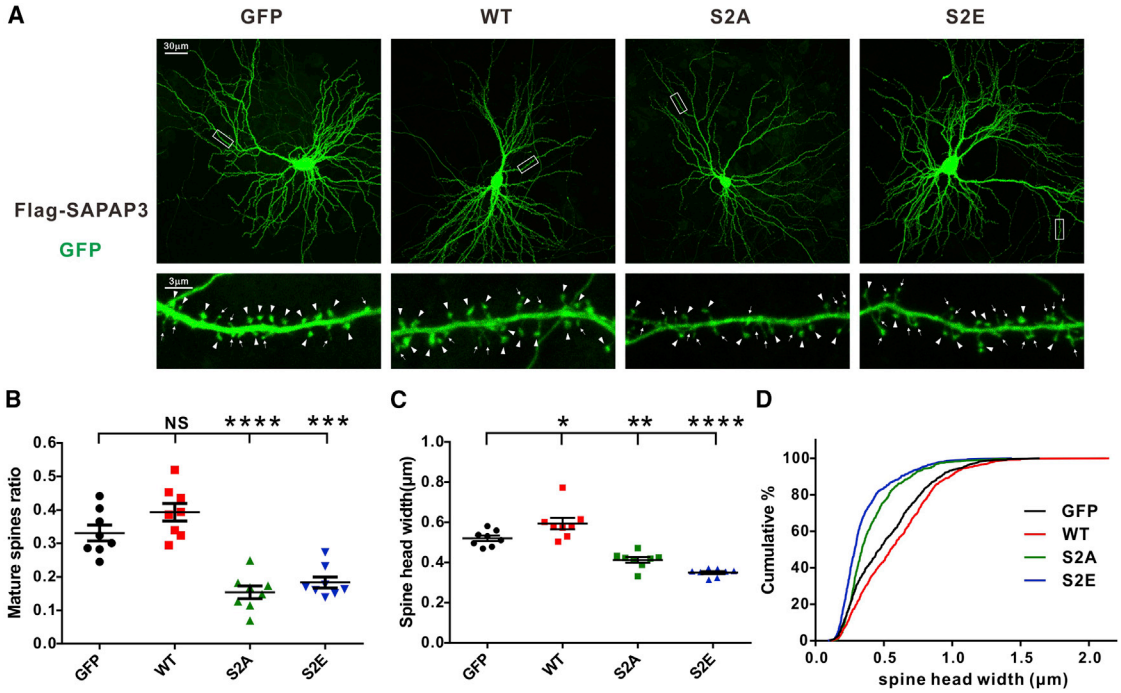

Figure 4. Overexpression of SAPAP3 S2A/S2E Mutants Leads to Defects in Dendritic Spine Development

(A) Representative images of transfected hippocampal neurons at DIV17. Arrowheads indicate mature spines with a mushroom-like head, and arrows represent immature spines including filopodia, branchy, stubby, and thin mushroom types of spines.

(B) Quantification of image data showing reduction of mature spines for the neurons expressed the SAPAP3 S2A and S2E mutants. Eight neurons (i.e., n = 8) from three independent batches of cultures were imaged for each group for quantifications. Error bar indicates ± SEM. ***p < 0.001, ****p < 0.0001; NS, not significant. One-way ANOVA with Tukey's multiple comparison test.

(C) Quantification of imaging data showing reduction in spine head width for the S2A and S2E SAPAP3 mutants expressing neurons. *p < 0.05, **p < 0.01, and ****p < 0.0001, one-way ANOVA with Tukey's multiple comparison test.

(D) Cumulative frequency plot of spine head width of neurons expressing various forms of SAPAP3.

dendritic spine development. Expression of the SAPAP3 S2A or SAPAP3 S2E mutants appears to have a dominant-negative effect on dendritic spine development in cultured neurons.

Disruption of the PSD-95/SAPAP Interaction by a Designed Non-phosphor Inhibitory Peptide

We next tried to evaluate the possible impact of disruption of the PSD-95/SAPAP interaction on synaptogenesis. Although the above-characterized phosphor-SAPAP peptides can be used to effectively block the PSD-95/SAPAP complex formation *in vitro*, they may not be effective tools for *in vivo* studies in neurons due to their poor cell penetration (Dunican and Doherty, 2001; Ye et al., 2007) and susceptibility of the phosphate group to removal by protein phosphatases in the cellular milieu. Another limitation of these phosphopeptides is that they cannot be genetically encoded for cellular or *in vivo* expressions. Furthermore, the phosphor-mimetic mutations of the SAPAP peptides are not effective in disrupting the PSD-95/SAPAP interaction either (Figure 2C). Therefore, we attempted to use the structural knowledge of the DLG GK/phosphopeptide interactions to design non-phosphopeptides that are capable of disrupting the PSD-95/SAPAP interaction.

Based on the sequence analysis of the DLG GK-binding phosphopeptides and the four DLG GK/phosphopeptide complex structures, the peptide-binding interface on GK can be arbitrarily separated into the following 7 sites (Xia et al., 2017; Zhu et al., 2011, 2014, 2016b; this study) (Figure 5A): (1) pSer site, which coordinates the phosphate group of phosphopeptides or the side chain of pSer-mimicking Glu/Asp of non-phosphopeptides; (2) the hydrophobic site formed by P564, Y580, Y604, and Y609 of GK, which accommodates $Y(+1)/A(+4)_{pSAPAP1\text{-}R2}$, $M(+1)/L(+4)_{pLGN}$, and $L(+1)/S(+4)_{pLgl2}$, respectively; (3) the hydrophobic cradle formed by I593, A601, and L608 of GK, which coordinates $M(+7)_{pLGN}$ or $F(+9)_{pLgl2}$; (4) an Asp residue cluster (D545, D549, and D629 of GK) coordinating with $R(-3)_{pSAPAP1\text{-}R2}$ or $K(+1)_{pLgl2}$; (5) the main chains of R578 and D579 of GK, which form hydrogen bonds with $R(-2)_{pLGN}$ or $R(-2)_{pSAPAP1\text{-}R2}$; (6) a hydrophobic pocket formed by L552 and I627 of GK; and (7) the positively charged R637 beneath the hydrophobic cradle of GK. It is noted that the pLGN and pLgl2 peptides utilize interactions between their C-terminal tails (i.e., residues beyond the +5 position) and site 3 of GK to enhance their bindings to GK (Zhu et al., 2011, 2014), and such interactions do not exist in the PSD-95/pSAPAP complex (Figures 2A and 2B). Thus, we reasoned that a chimeric phosphomimicking peptide that fuses the optimal SAPAP peptide with the C-terminal tails of the LGN peptide or Lgl2 peptide would enhance the chimeric SAPAP peptide's binding to PSD-95 GK.

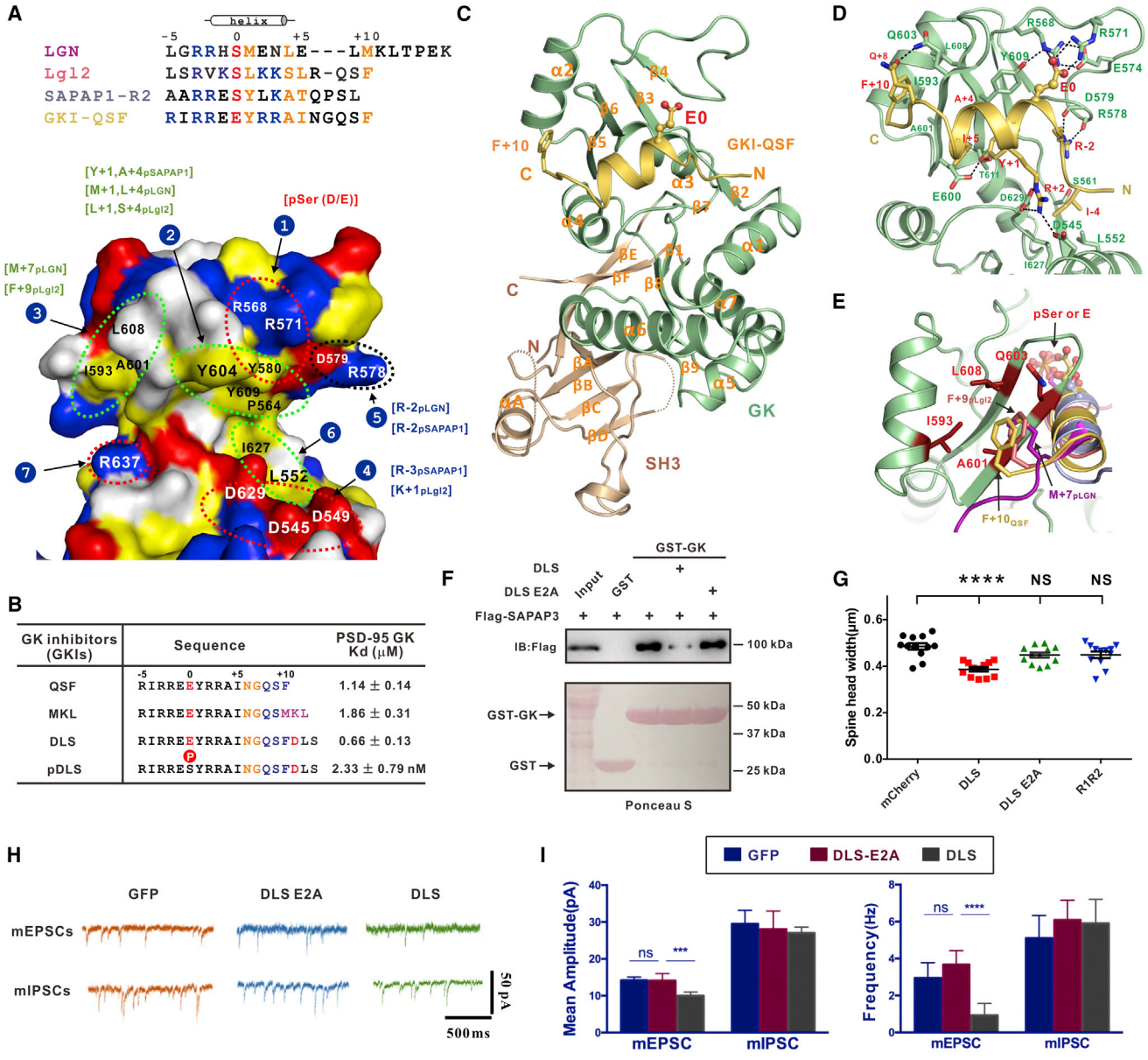

Figure 5. Designed Non-phosphopeptide Inhibitors of GK Effectively Block the PSD-95/SAPAP Interaction and Modulate Synaptogenesis

(A) Structure-based sequence alignment of known targets of DLG GKs. The phosphorylated Serines are color in red and positioned as "0" (top). The positively charged and hydrophobic residues are color in blue and orange, respectively. The bottom panel showing the surface representation of the PSD-95 GK which consists of seven binding sites for its target proteins.

(B) Summary of ITC-based measurements of the binding affinities between designed GKIs and PSD-95 GK.

(C) Ribbon diagram representation of the crystal structure of PSD-95 SH3-GK in complex with the GKI-QSF peptide. The side chain of E0 of the GKI-QSF peptide is shown in the ball-and-stick model. The side chain of $F(+10)_{QSF}$ is also shown.

(D) Detailed interactions between PSD-95 GK and the QSF peptide. Dotted lines denote hydrogen bonds and salt bridge interactions.

(E) Superposition of structures of GK/pLGN (PDB: 3UAT), GK/pLgl2 (PDB: 3WP0), and GK/GKI-QSF (this study) showing that the side chain of F(+10) in the designed QSF peptide occupies a very similar position on the Site-3 of GK as $M(+7)_{pLGN}$ and $F(+9)_{pLgl2}$ do in their complex with DLG GK.

(F) Pull-down-based competition experiment showing that the DLS peptide can effectively disrupt the PSD-95 GK/SAPAP3 interaction, whereas the DLS E2A mutant incapable of binding to PSD-95 GK cannot.

(G) Quantification of spine head width for neurons overexpressing designed GFP-fused peptides. Twelve neurons (i.e., n = 12) from four independent batches of cultures were imaged for each group for quantifications. Error bar indicates ± SEM. ****p < 0.0001; NS, not significant, using one-way ANOVA with Tukey's multiple comparison test.

(legend continued on next page)

Accordingly, the following three chimeric phosphomimicking GK inhibitory peptides (referred to as GKIs) were designed: QSF, RIRREEYRRANGQSF; MKL, RIRREEYRRANGQSMKL; and DLS, RIRREEYRRANGQSFDLS (Figure 5B). The designing strategy was as follows: a bulky hydrophobic Ile was used to substitute A(−4) of SAPAP-R2 for targeting site 6 of GK, and an Arg was placed at the −5 position for possible favorable interaction with the negatively charged residues in site 4 of GK (Figure 5A); a more bulky Ile was used to substitute T(+5) of SAPAP-R2 for better binding to the hydrophobic site (i.e., site 2) of GK; and the three different C-terminal tail sequences were designed to target the hydrophobic cradle (i.e., site 3) of GK that is not used by the pSAPAP-R2 peptide (Figure 2) but is engaged by the pLGN or pLgl2 peptides (Figure 5E). A two-residue linker ("NG") was used to connect the C-terminal tail with the optimal SAPAP-R2. Satisfyingly, ITC-based assays revealed that these non-phosphorylated GKI peptides bound to PSD-95 GK with K_d values ranging from 0.66 to 1.86 μM (Figure 5A). Notably, the DLS peptide bound to GK with a stronger affinity than other GKIs did, which was probably due to additional interaction between $D(+11)_{DLS}$ and R637 in site 7 of GK (Figure 5A). One would expect that the phosphorylated GKIs would have even stronger binding to PSD-95 GK. Indeed, the phosphorylated DLS peptide (pDLS) bound to PSD-95 GK with a super strong binding affinity (K_d ~2 nM) (Figure 5B). Taken together, the above biochemical data indicate that the strategy we used to design specific GKIs works well.

To further rationalize the enhanced GK bindings of these GKIs, we tried to crystallize various GKIs in complex with PSD-95 GK or SH3-GK. We were able to obtain the high-diffraction-quality crystals of the PSD-95 SH3-GK/QSF peptide complex, and we solved the structure at 2.35-Å resolution (Table S1). In the complex, the residues from E(0) to I(+5) of the QSF peptide formed an expected α-helical structure binding to site 1 and site 2 on GK. The carboxyl group of E(0) interacted with R568, R571, and Y609 in a way similar to that of pSer (Figures 5C and 5E). In agreement with our design strategy, $I(-4)_{QSF}$ interacted with hydrophobic residues in site 6 of GK (Figure 5D; Figure S1A). Somewhat surprisingly, the side chain of $R(+2)_{QSF}$ occupied the same position as the side chain of $R(-3)_{pSAPAP1\text{-}R2}$ did by forming salt bridges with the side chains of D545 and D549 (site 4) of GK (Figures 5A and 5D; Figure S1A). Most notably, the side chain of $F(+10)_{QSF}$ coupled with the hydrophobic cradle (site 3) of GK in a manner similar to that of $M(+7)_{pLGN}$ or $F(+9)_{pLgl2}$ in their respective complex with GK (Figures 5A, 5D, and 5E; Figure S1A). We believe that F(+10) plays a critical role in enhancing the binding of the QSF peptide to PSD-95 GK. In line with these structural analyses, substitution of $E(0)_{QSF}$ with Ala dramatically weakened its binding to PSD-95 GK; substitution of A601 in the shallow hydrophobic cradle of GK accommodating $F(+10)_{QSF}$ with Asp also decreased PSD-95 GK's binding to the QSF peptide by ~4-fold (Figures S1B–S1D).

We next tested whether these GKIs can block the PSD-95/SAPAP interaction *in vitro*. Since the DLS peptide binds to PSD-95 GK with the strongest binding affinity, we thus chose the DLS peptide for further study. As expected, glutathione S-transferase (GST)-tagged PSD-95 GK could robustly pull down FLAG-tagged SAPAP3 expressed in heterologous cells (Figure 5F, lane 3). Addition of the DLS peptide in the reaction mixture significantly reduced the interaction between PSD-95 GK and SAPAP3 (Figure 5F, lane 4), whereas the DLS E2A mutant peptide (i.e., substituting E(0) with Ala; also see Figure S1D) had no impact on the binding (Figure 5F, lane 5), further confirming the specificity of the DLS peptide in blocking the PSD-95/SAPAP interaction.

Given that the DLS peptide can effectively block the PSD-95/SAPAP interaction *in vitro*, we next investigated whether this peptide can effectively modulate the synaptogenesis when expressed in neurons. In this assay, GFP-DLS, GFP-DLS E2A, and GFP-R1R2 (SAPAP3 fragment containing two GBR motifs) were individually co-transfected with mCherry into cultured hippocampal neurons (DIV14). mCherry alone was also transfected as a control. At DIV17, all groups of neurons were fixed and analyzed for dendritic spine morphology. Neurons expressing the DLS peptide showed a significant decrease of spine head width compared with those expressing mCherry alone, the DLS E2A peptide, or the R1R2 peptide (Figure 5G; Figure S2; mCherry = 0.48 ± 0.01 μm, DLS = 0.39 ± 0.01 μm, E2A = 0.45 ± 0.01 μm, and R1R2 = 0.45 ± 0.01 μm; ****$p < 0.0001$, one-way ANOVA with Tukey's multiple comparison test; R1R2 peptide: a SAPAP3 fragment containing two GBR motifs in tandem), indicating that blocking the synaptic PSD-95/SAPAP interaction can interfere with dendritic spine development in cultured neurons.

We further investigated whether the DLS peptide can effectively modulate synaptic activity. EGFP-fused DLS peptide, the GFP-fused control peptide DLS-E2A, and GFP alone were expressed in the CA1 region of the dorsal hippocampus of adult mice using Lenti-DLS-GFP, Lenti-DLS-E2A-GFP, and Lenti-GFP virus vectors, respectively (Figure S3). The miniature excitatory postsynaptic currents (mEPSCs) and miniature inhibitory postsynaptic currents (mIPSCs) from CA1 pyramidal neurons in the hippocampal slices expressing GFP, GFP-DLS-E2A, or GFP-DLS were recorded using whole-cell patch-clamp techniques (Figures 5H and 5I). Both the amplitudes and frequencies of mEPSCs in neurons expressing DLS were significantly reduced compared with those expressing either GFP or the GFP-DLS-E2A control (Figure 5I). In contrast, the mIPSCs in neurons expressing DLS-GFP did not differ from those expressing either GFP or GFP-DSL-E2A (Figure 5I). These data indicate that the delivery of the DLS peptide into neurons specifically weakens the excitatory synaptic strength and acts most likely through disrupting the synaptic PSD-95/SAPAP interaction.

(H) Representative recordings of the miniature EPSCs (mEPSCs) and miniature IPSCs (mIPSCs) from CA1 pyramidal neurons in the hippocampal slices expressing GFP, GFP-DLS-E2A, or GFP-DLS.

(I) The mean amplitudes (left) and the frequencies (right) of mEPSCs and mIPSCs are shown in bar graphs. Data are presented as mean ± SEM using Student's t test. (n = 9 recordings/4 mice/group; ***$p < 0.001$ and ****$p < 0.0001$).

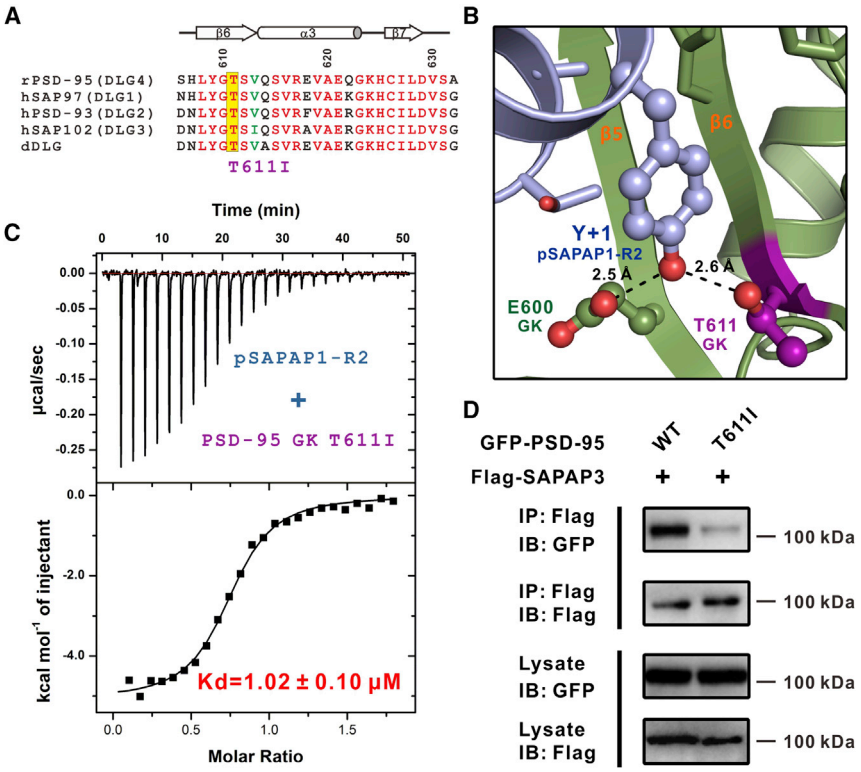

Figure 6. The Effect of ID-Associated PSD-95 T611I Mutation on the Formation of the PSD-95/SAPAP Complex

(A) The structure-based sequence alignment showing that T611 is totally conserved among all members of the DLG family MAGUKs. In this alignment, the absolutely conserved and conserved residues are color in red and green, respectively. The conserved T611 residues are highlighted with a yellow box.

(B) The combined ribbon and ball-and-stick representations showing that the side chain of ID-associated PSD-95 T611 residue, together with the side chain of PSD-95 E600, forms hydrogen bond network with the absolutely conserved Tyr at the +1 position of the pSAPAP1-R2 peptide.

(C) The ITC-based measurement of the binding affinity of the PSD-95 GK-T611I/pSAPAP1-R2 interaction.

(D) CoIP assay showing that T611I mutant of PSD-95 weakens the PSD-95/SAPAP binding.

Mechanistic Insights into an ID-Associated Mutation in PSD-95 GK

PSD-95 has been associated with a variety of brain disorders, including ID, schizophrenia, and ASD (Balan et al., 2013; Feyder et al., 2010; Lelieveld et al., 2016; Nithianantharajah et al., 2013). We noted with interest that a missense mutation of PSD-95 (T611I) was identified by a large-scale exome sequencing of patients with ID (Rauch et al., 2012). Sequence alignment analysis showed that T611 was absolutely conserved among the DLG family of MAGUKs (Figure 6A). On the basis of the PSD-95 GK/pSAPAP1-R2 complex structure solved in this study, $T611_{PSD-95}$ locates in the binding interface between GK and pSAPAP, and the side chain of T611 forms a hydrogen bond with Y(+1) of pSAPAP1-R2 (Figure 6B). Therefore, substitution of T611 with Ile was expected to affect the PSD-95/pSAPAP interaction. Indeed, the T611I mutant of PSD-95 GK showed an ~12-fold decrease of binding to pSAPAP1-R2 (Figure 6C; Figure 2C). CoIP assay also demonstrated that T611I mutation significantly decreased the interaction between the full-length PSD-95 and the full-length SAPAP3 (Figure 6D). Given that the tight and specific interaction between PSD-95 and SAPAPs is important for synapse development and maturation, our structural and biochemical data provide a mechanistic explanation of why the T6611I mutation of PSD-95 found in patients may interfere with synapse development and cause ID.

DISCUSSION

The PSD-95/SAPAP/Shank complex plays vital roles in synaptic development and activities by interfacing the glutamate receptors on the synaptic plasma membranes and actin cytoskeleton at the deeper layer of PSD. Recently, we discovered an exquisitely strong binding mode between Shank and SAPAP that determines the highly specific Shank/SAPAP complex formation as well as targeting of Shank to synapses (Zeng et al., 2016). In the present study, we provide biochemical and structural evidence showing that the interaction between PSD-95 and SAPAP is also very strong and specific (K_d in the range of a few dozens of nanomolar). Most importantly, we demonstrate that the specific interaction between PSD-95 and SAPAPs is phosphorylation dependent. Phosphorylation of a highly conserved Ser residue in each GBR motif of SAPAPs switches on the interaction between PSD-95 and SAPAPs. Removal of the phosphate group from the Ser in GBR eliminates the binding of SAPAPs to PSD-95 (Figure 1). We also provide evidence to show that the phosphorylation-dependent PSD-95/SAPAP interaction is required for SAPAP's synaptic targeting and dendritic spine development (Figures 3 and 4). These findings indicate that the formation of the PSD-95/SAPAP complex in PSD is regulated by synaptic activities, providing an avenue for dynamic regulation of PSD assemblies. It is envisioned that changes of synaptic activity and ensuing alterations of protein kinase/phosphatase activity can modulate phosphorylation status of the GBR motifs in SAPAPs and, thus, regulate the formation of the PSD-95/SAPAP complex.

Our above finding immediately raises a number of questions: (1) Are SAPAPs phosphorylated *in vivo* and to what extent are SAPAPs phosphorylated? (2) Which kinase(s) phosphorylates SAPAPs? (3) Which phosphatase(s) acts to remove the phosphorylation? (4) How are the activities of the kinase(s) and phosphatase(s) coordinated with synaptic signals? Proteomic studies have indicated that SAPAPs are indeed phosphorylated *in vivo* (Collins et al., 2005; Trinidad et al., 2005, 2008). Moreover, the GBR motifs of SAPAPs have been shown to be phosphorylated by CaMKII directly *in vitro* and in cultured neurons (Collins et al.,

2005; Shin et al., 2012; Trinidad et al., 2005), thus linking the key synaptic activity regulatory kinase with the PSD-95/SAPAP complex formation. It is noted that the consensus sequence (-R-x-x-S-Y-x-x-A-) from the GBR motifs of SAPAPs fits well with the substrate recognition sequences of other kinases, including protein kinase A (PKA), protein kinase C (PKC), and protein kinase D (PKD) (Ubersax and Ferrell, 2007; Wang et al., 2012); it is tempting to speculate that SAPAPs might also be phosphorylated by these kinases in synapses. CaMKII, PKA, and PKC are all known to be tightly associated with synaptic development and plasticity via phosphorylating a wide spectrum of synaptic proteins (Boehm et al., 2006; Okamoto et al., 2009; Zhong et al., 2009). Therefore, the phosphorylation-dependent PSD-95/SAPAP interaction can, in principle, provide a regulated switch of assembly/disassembly of PSD components, which is likely coupled to synaptic activity changes. Future work is required to validate whether the direct coupling between regulated PSD-95/SAPAP-mediated PSD assembly and dynamic changes in synaptic activity is indeed present in neurons and, if the answer is yes, how such coupling is modulated via synaptic activity-dependent modulations of specific kinases and phosphatases.

Mammals contain four paralogs of DLGs and four SAPAPs. The existence of multiple highly homologous paralogs of these two major PSD scaffold proteins have posed major challenges in investigating their roles in synaptic development and functions, in large part due to compensatory effects among the members. It is desirable to develop tools that can specifically modulate the interactions between the DLG family and the SAPAP family proteins for studying their functional roles in synapses under both physiological and pathological conditions. Based on the structures of DLG GK/target complexes elucidated in this work and our earlier studies, we successfully designed a non-phosphopeptide that can specifically inhibit the formation of the PSD-95/SAPAP complex (Figure 5A). Given that the GK domains of DLGs share essentially the same phosphopeptide-binding property (Zhu et al., 2011, 2014) and the SAPAPs contain highly conserved GBR motifs, our developed GKI is expected to be able to block the complex formation between all paralogs of the DLG family and the SAPAP family proteins. Our developed GKI does not require Ser(0) in GBR motifs to be phosphorylated, and thus it should be more stable when delivered to living neurons. Perhaps most importantly, such non-phosphopeptide can be genetically encoded and paired with any tagging sequences, such as fluorescence proteins or specific cellular targeting motifs, for various cell biology studies of the functions of the DLG/SAPAP interactions. We have provided a proof-of-concept use of such inhibitory peptide by studying their impact on the synaptic targeting of SAPAPs and synaptogenesis and synaptic activity using neuronal culture as well as brain slice culture as the models (Figure 5). We note that the binding affinity of the best GKI (the DLS peptide; Figure 5), although with a K_d value at a sub-micromolar range, is still about 10-fold lower than the naturally occurring phosphor-GBR motif peptides (Figures 5B and 2C). Further work is required to develop GKIs with even higher binding affinities to the DLG GK domains.

Finally, the structure of the PSD-95 GK/pSAPAP1-R2 complex determined in this study, together with our systematic biochemical investigations, not only elucidates the mechanistic basis governing the phosphorylation-dependent PSD-95/SAPAP complex formation but also provides a foundation for understanding why certain mutations of the genes encoding the two major scaffold proteins may cause neuronal diseases in humans.

EXPERIMENTAL PROCEDURES

Protein Expression and Purification

Preparations of the rat PSD-95 GK domain (amino acid residues 531–713; NCBI sequence: NP_062567) and various mutants followed the previously described methods (Zhu et al., 2011, 2014). All the phosphor- or non-phosphor-SAPAP peptides and the GKIs were commercially synthesized (China Peptides).

ITC Assay

ITC measurements were performed on a MicroCal iTC200 system (Malvern) in a buffer containing 50 mM Tris (pH 8.0), 100 mM NaCl, 1 mM EDTA, and 1 mM DTT at 25°C. The concentrations of proteins loaded into the syringe and the cell were 0.5 and 0.05 mM, respectively. The titration data were analyzed using Origin7.0 from MicalCal and fitted by a one-site binding model. The error on each K_d value represents the SE for the fit of the curve from each titration experiment. The summary of parameters of ITC assays in this study are listed in Table S2.

Protein Crystallization and Structure Determination

Crystals of the PSD-95 GK/pSAPAP1-R2 complex and the PSD-95 SH3-GK/GKI-QSF complex were obtained by the hanging drop vapor diffusion method at 16°C. The PSD-95 GK/pSAPAP1-R2 complex crystals were grown in 0.1 M ammonium acetate, 0.1 M Bis-Tris (pH 5.5), and 17% w/v polyethylene glycol 10,000. The PSD-95 SH3-GK/GKI-QSF complex crystals were grown in 0.1 M Tris (pH 8.0) and 35% tert-butanol; 25% glycerol was added as the cryo-protectant before diffraction data collection. The structures were both solved by the molecular replacement method using PSD-95 SH3-GK structure (PDB: 1KJW) as the search model with Phaser (McCoy et al., 2007) in CCP4 (Murshudov et al., 2011). Refinements were carried out using phenix.refinement (Adams et al., 2010). The pSAPAP-R2 peptides and the GKI-QSF peptide were manually built. Further model buildings and adjustment were completed using Coot (Emsley et al., 2010). The structural diagrams were prepared by the program PyMOL (www.pymol.org).

CoIP Assay and GST Pull-Down Assay

For coIP assays, FLAG-tagged SAPAP3 and GFP-tagged PSD-95 and their various mutants were co-expressed in HEK293T cells. After 24 hr of transfection, cells were lysed in the ice-cold cell lysis buffer containing 50 mM HEPES (pH 7.4), 150 mM NaCl, 10% glycerol, 1 mM EGTA, 1% Triton, and protease inhibitor cocktail for 1 hr at 4°C, followed by centrifugation at 12,000 rpm for 10 min at 4°C. In each reaction, the supernatant was incubated with 20 μL anti-FLAG M2 magnetic beads (Sigma-Aldrich) for 1 hr at 4°C. After extensive washing, the captured proteins were separated by SDS-PAGE and detected by western blot using specific antibodies.

For the GST pull-down assay, HEK293T cells expressing the FLAG-tagged SAPAP3 were lysed in the ice-cold cell lysis buffer, followed by centrifugation at 12,000 rpm for 10 min at 4°C. The supernatant was incubated with 20 μL glutathione Sepharose beads loaded with GST-GK with or without GKIs for 2 hr at 4°C. After extensive washing, the captured proteins were separated by SDS-PAGE and detected by western blot using anti-FLAG antibody (Sigma).

Primary Hippocampal Neuron Culture

Hippocampal neuron cultures were prepared as previously described (Zeng et al., 2016). At DIV14, neurons were transfected with 2 μg plasmids per well (12-well plate) using Lipofectamine 2000 reagent (Invitrogen). Neurons were fixed at DIV17 with 4% paraformaldehyde (PFA) together with 4% sucrose in 1×PBS buffer and mounted on slides for imaging.

Image Acquisition and Quantification

Confocal images were obtained using a Leica SP8 confocal microscope with a 40× oil-immersion lens. Transfected neurons were chosen randomly for quantification from at least three independent batches of cultures. For detailed spine visualization, an additional 5× zoom factor was applied. Normally, four randomly selected dendrites (~60 μm in length each) were imaged and analyzed from an individual neuron. Each image was collected as a z series maxim projection with 0.35-μm depth intervals. Intensity and spine head width were measured with ImageJ.

Stereotaxic Injection

Mice (C57BL/6, 4–5 weeks old, male) were anesthetized with isoflurane (2%–5%) and then placed in a stereotaxic device where the head was fixed and the skull was exposed. Burr holes were made, and a microsyringe (World Precision Instruments) was slowly lowered into the dorsal CA1 at 2.06 mm anteroposterior, 1.38 mm mediolateral, and 1.60 mm dorsoventral relative to bregma. For the electrophysiological experiments, 200 nL virus was pressure-injected into each hemisphere. The syringe remained in place for 5 min and was then slowly retracted out. The mice were placed on a heating pad during the surgery. After virus injection, the scalp was sutured and saline was administered subcutaneously. The mice were placed on the heating pad during recovery from anesthesia. The electrophysiological experiments were conducted 2 weeks after the virus injection. Mice were bred and reared under the conditions in accordance with institutional guidelines and the Animal Care and Use Committee of the animal core facility at Huazhong University of Science and Technology, Wuhan, China.

Electrophysiology

Hippocampal slices (300 μm) were prepared as described previously (Tu et al., 2010). The slices were transferred to a holding chamber that contains artificial cerebrospinal fluid (in mM: 124 NaCl, 3 KCl, 26 $NaHCO_3$, 1.25 NaH_2PO_4, 1.2 $MgCl_2$, 10 $C_6H_{12}O_6$, and 2 $CaCl_2$ [pH 7.4], 305 mOsm). The slices were allowed to recover at 31.5°C for 30 min and then at room temperature for 1 hr. Acute slices were transferred to a recording chamber continuously, which was perfused with oxygenated artificial cerebrospinal fluid (2 mL/min) and maintained at room temperature. For whole-cell patch-clamp recordings from the CA1 pyramidal cells, hippocampal slices were visualized via IR-DIC by using an Axioskop 2FS equipped with Hamamatsu C2400-07E optics (Hamamatsu City, Japan). Basic electrophysiological properties were recorded when stable recordings were achieved with good access resistance (~20 MΩ). The mEPSCs were recorded using an internal solution containing (in mM) 140 potassium gluconate, 10 HEPES, 0.2 EGTA, 2 MgATP, 2 NaCl, and 0.3 NaGTP and an external solution containing 10 μM bicuculline and 1 μM tetrodotoxin (TTX). The mIPSCs were recorded with an internal solution containing (in mM) 153.3 CsCl,1 $MgCl_2$, 5 EGTA, 10 HEPES, 4 MgATP and an external solution containing 10 μM 6-cyano-7-nitroquinoxaline-2,3-dione (CNQX), 50 μM APV, and 1 μM TTX. The data were collected at 10 kHz and filtered with a low-pass filter at 2 kHz. Miniature events were analyzed in Clampfit 10.2 software (Molecular Devices, Sunnyvale, CA, USA) using template matching and a threshold of 5 pA.

DATA AND SOFTWARE AVAILABILITY

The accession numbers for the atomic coordinates of the PSD-95 GK/pSAPAP1-R2 complex and of the PSD-95 SH3-GK/QSF complex reported in this paper are PDB: 5YPO and 5YPR, respectively.

SUPPLEMENTAL INFORMATION

Supplemental Information includes three figures and two tables and can be found with this article online at https://doi.org/10.1016/j.celrep.2017.11.107.

ACKNOWLEDGMENTS

We thank the Shanghai Synchrotron Radiation Facility (SSRF) BL17U, BL18U, and BL19U1 for X-ray beam time and the National Centre for Protein Science Shanghai for their instrument support and technical assistance. This work was supported by grants from the National Natural Science Foundation of China (31770779, 31470733, and U1532121), a grant from Shanghai Municipal Science and Technology Commission, China (Yang-Fan program, 14YF1406700), and an SA-SIBS scholarship program to J.Z.; grants from RGC of Hong Kong (16103614, 16149516, and AoE-M09-12) to M.Z. and (C6009-15G) to M.Z. and X.H.; and a 973 program grant from the Minister of Science and Technology of China (2014CB910204) to M.Z. M.Z. is a Kerry Holdings Professor in Science and a Senior Fellow of IAS at HKUST.

AUTHOR CONTRIBUTIONS

J.Z., Q.Z., and M.Z. designed the experiments. J.Z., Q.Z., Y.S., M.P., and Z.W. performed biochemical and structural biology experiments. Q.Z. performed neuronal cell biology experiments. Y.S., X.H., and S.S.C.L. performed inhibitory peptide design and optimization experiments. H.L. and X.K. performed electrophysiology experiments. J.Z., R.Z., G.F., Y.L., and M.Z. analyzed the data. J.Z., Q.Z., and M.Z. wrote the manuscript. M.Z. coordinated the research.

DECLARATION OF INTERESTS

The authors declare no competing interests.

Received: September 20, 2017
Revised: November 13, 2017
Accepted: November 29, 2017
Published: December 26, 2017

REFERENCES

Adams, P.D., Afonine, P.V., Bunkóczi, G., Chen, V.B., Davis, I.W., Echols, N., Headd, J.J., Hung, L.-W., Kapral, G.J., Grosse-Kunstleve, R.W., et al. (2010). PHENIX: a comprehensive Python-based system for macromolecular structure solution. Acta Crystallogr. D Biol. Crystallogr. *66*, 213–221.

Balan, S., Yamada, K., Hattori, E., Iwayama, Y., Toyota, T., Ohnishi, T., Maekawa, M., Toyoshima, M., Iwata, Y., Suzuki, K., et al. (2013). Population-specific haplotype association of the postsynaptic density gene DLG4 with schizophrenia, in family-based association studies. PLoS ONE *8*, e70302.

Bayés, A., and Grant, S.G. (2009). Neuroproteomics: understanding the molecular organization and complexity of the brain. Nat. Rev. Neurosci. *10*, 635–646.

Bienvenu, O.J., Wang, Y., Shugart, Y.Y., Welch, J.M., Grados, M.A., Fyer, A.J., Rauch, S.L., McCracken, J.T., Rasmussen, S.A., Murphy, D.L., et al. (2009). Sapap3 and pathological grooming in humans: Results from the OCD collaborative genetics study. Am. J. Med. Genet. B. Neuropsychiatr. Genet. *150B*, 710–720.

Boehm, J., Kang, M.G., Johnson, R.C., Esteban, J., Huganir, R.L., and Malinow, R. (2006). Synaptic incorporation of AMPA receptors during LTP is controlled by a PKC phosphorylation site on GluR1. Neuron *51*, 213–225.

Carlin, R.K., Grab, D.J., Cohen, R.S., and Siekevitz, P. (1980). Isolation and characterization of postsynaptic densities from various brain regions: enrichment of different types of postsynaptic densities. J. Cell Biol. *86*, 831–845.

Chen, X., Winters, C., Azzam, R., Li, X., Galbraith, J.A., Leapman, R.D., and Reese, T.S. (2008). Organization of the core structure of the postsynaptic density. Proc. Natl. Acad. Sci. USA *105*, 4453–4458.

Chen, X., Levy, J.M., Hou, A., Winters, C., Azzam, R., Sousa, A.A., Leapman, R.D., Nicoll, R.A., and Reese, T.S. (2015). PSD-95 family MAGUKs are essential for anchoring AMPA and NMDA receptor complexes at the postsynaptic density. Proc. Natl. Acad. Sci. USA *112*, E6983–E6992.

Collins, M.O., Yu, L., Coba, M.P., Husi, H., Campuzano, I., Blackstock, W.P., Choudhary, J.S., and Grant, S.G. (2005). Proteomic analysis of in vivo phosphorylated synaptic proteins. J. Biol. Chem. *280*, 5972–5982.

Crane, J., Fagerness, J., Osiecki, L., Gunnell, B., Stewart, S.E., Pauls, D.L., and Scharf, J.M.; Tourette Syndrome International Consortium for Genetics

(TSAICG) (2011). Family-based genetic association study of DLGAP3 in Tourette syndrome. Am. J. Med. Genet. B. Neuropsychiatr. Genet. *156B*, 108–114.

Dieterich, D.C., and Kreutz, M.R. (2016). Proteomics of the synapse–a quantitative approach to neuronal plasticity. Mol. Cell. Proteomics *15*, 368–381.

Dunican, D.J., and Doherty, P. (2001). Designing cell-permeant phosphopeptides to modulate intracellular signaling pathways. Biopolymers *60*, 45–60.

Elias, G.M., and Nicoll, R.A. (2007). Synaptic trafficking of glutamate receptors by MAGUK scaffolding proteins. Trends Cell Biol. *17*, 343–352.

Emsley, P., Lohkamp, B., Scott, W.G., and Cowtan, K. (2010). Features and development of Coot. Acta Crystallogr. D Biol. Crystallogr. *66*, 486–501.

Feyder, M., Karlsson, R.M., Mathur, P., Lyman, M., Bock, R., Momenan, R., Munasinghe, J., Scattoni, M.L., Ihne, J., Camp, M., et al. (2010). Association of mouse Dlg4 (PSD-95) gene deletion and human DLG4 gene variation with phenotypes relevant to autism spectrum disorders and Williams' syndrome. Am. J. Psychiatry *167*, 1508–1517.

Fukata, Y., Dimitrov, A., Boncompain, G., Vielemeyer, O., Perez, F., and Fukata, M. (2013). Local palmitoylation cycles define activity-regulated postsynaptic subdomains. J. Cell Biol. *202*, 145–161.

Grant, S.G. (2012). Synaptopathies: diseases of the synaptome. Curr. Opin. Neurobiol. *22*, 522–529.

Hirao, K., Hata, Y., Ide, N., Takeuchi, M., Irie, M., Yao, I., Deguchi, M., Toyoda, A., Sudhof, T.C., and Takai, Y. (1998). A novel multiple PDZ domain-containing molecule interacting with N-methyl-D-aspartate receptors and neuronal cell adhesion proteins. J. Biol. Chem. *273*, 21105–21110.

Hung, A.Y., Futai, K., Sala, C., Valtschanoff, J.G., Ryu, J., Woodworth, M.A., Kidd, F.L., Sung, C.C., Miyakawa, T., Bear, M.F., et al. (2008). Smaller dendritic spines, weaker synaptic transmission, but enhanced spatial learning in mice lacking Shank1. J. Neurosci. *28*, 1697–1708.

Jiang-Xie, L.F., Liao, H.M., Chen, C.H., Chen, Y.T., Ho, S.Y., Lu, D.H., Lee, L.J., Liou, H.H., Fu, W.M., and Gau, S.S. (2014). Autism-associated gene Dlgap2 mutant mice demonstrate exacerbated aggressive behaviors and orbitofrontal cortex deficits. Mol. Autism *5*, 32.

Johnston, C.A., Doe, C.Q., and Prehoda, K.E. (2012). Structure of an enzyme-derived phosphoprotein recognition domain. PLoS ONE *7*, e36014.

Kim, E., and Sheng, M. (2004). PDZ domain proteins of synapses. Nat. Rev. Neurosci. *5*, 771–781.

Kim, E., Naisbitt, S., Hsueh, Y.P., Rao, A., Rothschild, A., Craig, A.M., and Sheng, M. (1997). GKAP, a novel synaptic protein that interacts with the guanylate kinase-like domain of the PSD-95/SAP90 family of channel clustering molecules. J. Cell Biol. *136*, 669–678.

Lelieveld, S.H., Reijnders, M.R., Pfundt, R., Yntema, H.G., Kamsteeg, E.J., de Vries, P., de Vries, B.B., Willemsen, M.H., Kleefstra, T., Löhner, K., et al. (2016). Meta-analysis of 2,104 trios provides support for 10 new genes for intellectual disability. Nat. Neurosci. *19*, 1194–1196.

Levy, J.M., Chen, X., Reese, T.S., and Nicoll, R.A. (2015). Synaptic consolidation normalizes AMPAR quantal size following MAGUK loss. Neuron *87*, 534–548.

MacGillavry, H.D., and Hoogenraad, C.C. (2015). The internal architecture of dendritic spines revealed by super-resolution imaging: What did we learn so far? Exp. Cell Res. *335*, 180–186.

MacGillavry, H.D., Song, Y., Raghavachari, S., and Blanpied, T.A. (2013). Nanoscale scaffolding domains within the postsynaptic density concentrate synaptic AMPA receptors. Neuron *78*, 615–622.

Marín, O. (2012). Interneuron dysfunction in psychiatric disorders. Nat. Rev. Neurosci. *13*, 107–120.

McCoy, A.J., Grosse-Kunstleve, R.W., Adams, P.D., Winn, M.D., Storoni, L.C., and Read, R.J. (2007). Phaser crystallographic software. J. Appl. Cryst. *40*, 658–674.

Murshudov, G.N., Skubák, P., Lebedev, A.A., Pannu, N.S., Steiner, R.A., Nicholls, R.A., Winn, M.D., Long, F., and Vagin, A.A. (2011). REFMAC5 for the refinement of macromolecular crystal structures. Acta Crystallogr. D Biol. Crystallogr. *67*, 355–367.

Nair, D., Hosy, E., Petersen, J.D., Constals, A., Giannone, G., Choquet, D., and Sibarita, J.B. (2013). Super-resolution imaging reveals that AMPA receptors inside synapses are dynamically organized in nanodomains regulated by PSD95. J. Neurosci. *33*, 13204–13224.

Naisbitt, S., Kim, E., Weinberg, R.J., Rao, A., Yang, F.C., Craig, A.M., and Sheng, M. (1997). Characterization of guanylate kinase-associated protein, a postsynaptic density protein at excitatory synapses that interacts directly with postsynaptic density-95/synapse-associated protein 90. J. Neurosci. *17*, 5687–5696.

Naisbitt, S., Kim, E., Tu, J.C., Xiao, B., Sala, C., Valtschanoff, J., Weinberg, R.J., Worley, P.F., and Sheng, M. (1999). Shank, a novel family of postsynaptic density proteins that binds to the NMDA receptor/PSD-95/GKAP complex and cortactin. Neuron *23*, 569–582.

Nithianantharajah, J., Komiyama, N.H., McKechanie, A., Johnstone, M., Blackwood, D.H., St Clair, D., Emes, R.D., van de Lagemaat, L.N., Saksida, L.M., Bussey, T.J., and Grant, S.G. (2013). Synaptic scaffold evolution generated components of vertebrate cognitive complexity. Nat. Neurosci. *16*, 16–24.

Okamoto, K., Bosch, M., and Hayashi, Y. (2009). The roles of CaMKII and F-actin in the structural plasticity of dendritic spines: a potential molecular identity of a synaptic tag? Physiology (Bethesda) *24*, 357–366.

Opazo, P., Sainlos, M., and Choquet, D. (2012). Regulation of AMPA receptor surface diffusion by PSD-95 slots. Curr. Opin. Neurobiol. *22*, 453–460.

Peça, J., Feliciano, C., Ting, J.T., Wang, W., Wells, M.F., Venkatraman, T.N., Lascola, C.D., Fu, Z., and Feng, G. (2011). Shank3 mutant mice display autistic-like behaviours and striatal dysfunction. Nature *472*, 437–442.

Pinto, D., Pagnamenta, A.T., Klei, L., Anney, R., Merico, D., Regan, R., Conroy, J., Magalhaes, T.R., Correia, C., Abrahams, B.S., et al. (2010). Functional impact of global rare copy number variation in autism spectrum disorders. Nature *466*, 368–372.

Rauch, A., Wieczorek, D., Graf, E., Wieland, T., Endele, S., Schwarzmayr, T., Albrecht, B., Bartholdi, D., Beygo, J., Di Donato, N., et al. (2012). Range of genetic mutations associated with severe non-syndromic sporadic intellectual disability: an exome sequencing study. Lancet *380*, 1674–1682.

Romorini, S., Piccoli, G., Jiang, M., Grossano, P., Tonna, N., Passafaro, M., Zhang, M., and Sala, C. (2004). A functional role of postsynaptic density-95-guanylate kinase-associated protein complex in regulating Shank assembly and stability to synapses. J. Neurosci. *24*, 9391–9404.

Sala, C., Piëch, V., Wilson, N.R., Passafaro, M., Liu, G., and Sheng, M. (2001). Regulation of dendritic spine morphology and synaptic function by Shank and Homer. Neuron *31*, 115–130.

Sheng, M., and Hoogenraad, C.C. (2007). The postsynaptic architecture of excitatory synapses: a more quantitative view. Annu. Rev. Biochem. *76*, 823–847.

Sheng, M., and Kim, E. (2011). The postsynaptic organization of synapses. Cold Spring Harb. Perspect. Biol. *3*, a005678.

Shin, S.M., Zhang, N., Hansen, J., Gerges, N.Z., Pak, D.T., Sheng, M., and Lee, S.H. (2012). GKAP orchestrates activity-dependent postsynaptic protein remodeling and homeostatic scaling. Nat. Neurosci. *15*, 1655–1666.

Stewart, S.E., Yu, D., Scharf, J.M., Neale, B.M., Fagerness, J.A., Mathews, C.A., Arnold, P.D., Evans, P.D., Gamazon, E.R., Davis, L.K., et al.; North American Brain Expression Consortium; UK Brain Expression Database (2013). Genome-wide association study of obsessive-compulsive disorder. Mol. Psychiatry *18*, 788–798.

Takeuchi, M., Hata, Y., Hirao, K., Toyoda, A., Irie, M., and Takai, Y. (1997). SAPAPs. A family of PSD-95/SAP90-associated proteins localized at postsynaptic density. J. Biol. Chem. *272*, 11943–11951.

Ting, J.T., Peça, J., and Feng, G. (2012). Functional consequences of mutations in postsynaptic scaffolding proteins and relevance to psychiatric disorders. Annu. Rev. Neurosci. *35*, 49–71.

Trinidad, J.C., Thalhammer, A., Specht, C.G., Schoepfer, R., and Burlingame, A.L. (2005). Phosphorylation state of postsynaptic density proteins. J. Neurochem. *92*, 1306–1316.

Trinidad, J.C., Thalhammer, A., Specht, C.G., Lynn, A.J., Baker, P.R., Schoepfer, R., and Burlingame, A.L. (2008). Quantitative analysis of synaptic phosphorylation and protein expression. Mol. Cell. Proteomics *7*, 684–696.

Tu, W., Xu, X., Peng, L., Zhong, X., Zhang, W., Soundarapandian, M.M., Balel, C., Wang, M., Jia, N., Zhang, W., et al. (2010). DAPK1 interaction with NMDA receptor NR2B subunits mediates brain damage in stroke. Cell *140*, 222–234.

Ubersax, J.A., and Ferrell, J.E., Jr. (2007). Mechanisms of specificity in protein phosphorylation. Nat. Rev. Mol. Cell Biol. *8*, 530–541.

Volk, L., Chiu, S.L., Sharma, K., and Huganir, R.L. (2015). Glutamate synapses in human cognitive disorders. Annu. Rev. Neurosci. *38*, 127–149.

Wang, C., Shang, Y., Yu, J., and Zhang, M. (2012). Substrate recognition mechanism of atypical protein kinase Cs revealed by the structure of PKCι in complex with a substrate peptide from Par-3. Structure *20*, 791–801.

Welch, J.M., Lu, J., Rodriguiz, R.M., Trotta, N.C., Peca, J., Ding, J.D., Feliciano, C., Chen, M., Adams, J.P., Luo, J., et al. (2007). Cortico-striatal synaptic defects and OCD-like behaviours in Sapap3-mutant mice. Nature *448*, 894–900.

Won, S., Levy, J.M., Nicoll, R.A., and Roche, K.W. (2017). MAGUKs: multifaceted synaptic organizers. Curr. Opin. Neurobiol. *43*, 94–101.

Xia, Y., Shang, Y., Zhang, R., and Zhu, J. (2017). Structure of the PSD-95/MAP1A complex reveals a unique target recognition mode of the MAGUK GK domain. Biochem. J. *474*, 2817–2828.

Ye, G., Nam, N.H., Kumar, A., Saleh, A., Shenoy, D.B., Amiji, M.M., Lin, X., Sun, G., and Parang, K. (2007). Synthesis and evaluation of tripodal peptide analogues for cellular delivery of phosphopeptides. J. Med. Chem. *50*, 3604–3617.

Zeng, M., Shang, Y., Guo, T., He, Q., Yung, W.H., Liu, K., and Zhang, M. (2016). A binding site outside the canonical PDZ domain determines the specific interaction between Shank and SAPAP and their function. Proc. Natl. Acad. Sci. USA *113*, E3081–E3090.

Zhong, H., Sia, G.M., Sato, T.R., Gray, N.W., Mao, T., Khuchua, Z., Huganir, R.L., and Svoboda, K. (2009). Subcellular dynamics of type II PKA in neurons. Neuron *62*, 363–374.

Zhu, J., Shang, Y., Xia, C., Wang, W., Wen, W., and Zhang, M. (2011). Guanylate kinase domains of the MAGUK family scaffold proteins as specific phospho-protein-binding modules. EMBO J. *30*, 4986–4997.

Zhu, J., Shang, Y., Wan, Q., Xia, Y., Chen, J., Du, Q., and Zhang, M. (2014). Phosphorylation-dependent interaction between tumor suppressors Dlg and Lgl. Cell Res. *24*, 451–463.

Zhu, J., Shang, Y., Xia, Y., Zhang, R., and Zhang, M. (2016a). An Atypical MAGUK GK Target Recognition Mode Revealed by the Interaction between DLG and KIF13B. Structure *24*, 1876–1885.

Zhu, J., Shang, Y., and Zhang, M. (2016b). Mechanistic basis of MAGUK-organized complexes in synaptic development and signalling. Nat. Rev. Neurosci. *17*, 209–223.

Züchner, S., Wendland, J.R., Ashley-Koch, A.E., Collins, A.L., Tran-Viet, K.N., Quinn, K., Timpano, K.C., Cuccaro, M.L., Pericak-Vance, M.A., Steffens, D.C., et al. (2009). Multiple rare SAPAP3 missense variants in trichotillomania and OCD. Mol. Psychiatry *14*, 6–9.

Cell Reports, Volume *21*

Supplemental Information

Synaptic Targeting and Function of SAPAPs Mediated by Phosphorylation-Dependent Binding to PSD-95 MAGUKs

Jinwei Zhu, Qingqing Zhou, Yuan Shang, Hao Li, Mengjuan Peng, Xiao Ke, Zhuangfeng Weng, Rongguang Zhang, Xuhui Huang, Shawn S.C. Li, Guoping Feng, Youming Lu, and Mingjie Zhang

Supplemental Figures

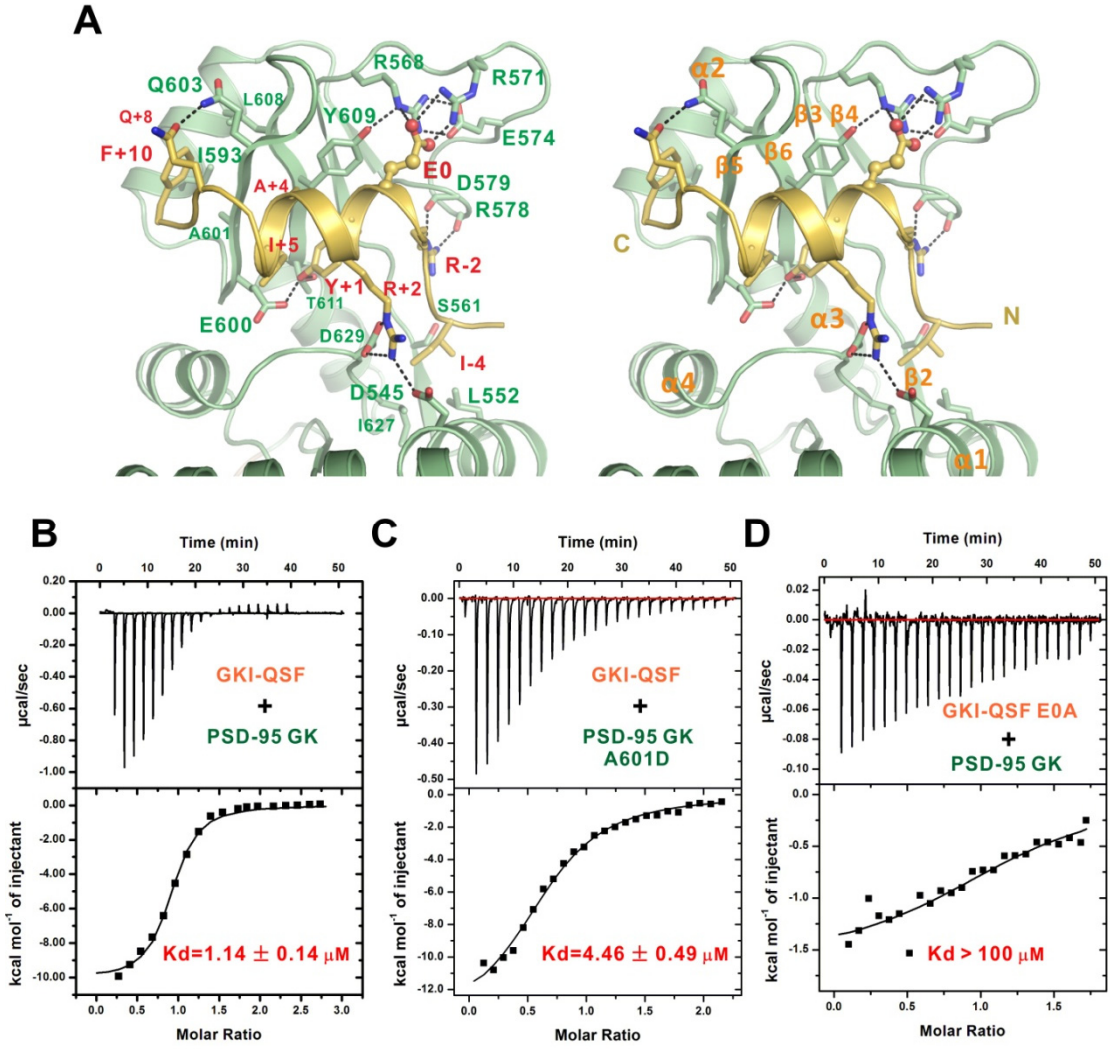

Figure S1. Detailed interface of PSD-95 SH3-GK/GKI-QSF complex and validation of the complex structure. Related to Fig. 5.

(A) Stereo view of detailed interaction between PSD-95 SH3-GK and the GKI-QSF peptide. Dotted lines denote hydrogen bonds and salt bridge interactions. **(B)** ITC-based measurements of binding affinities between wild-type and mutants of PSD-95 GK and the GKI-QSF peptide.

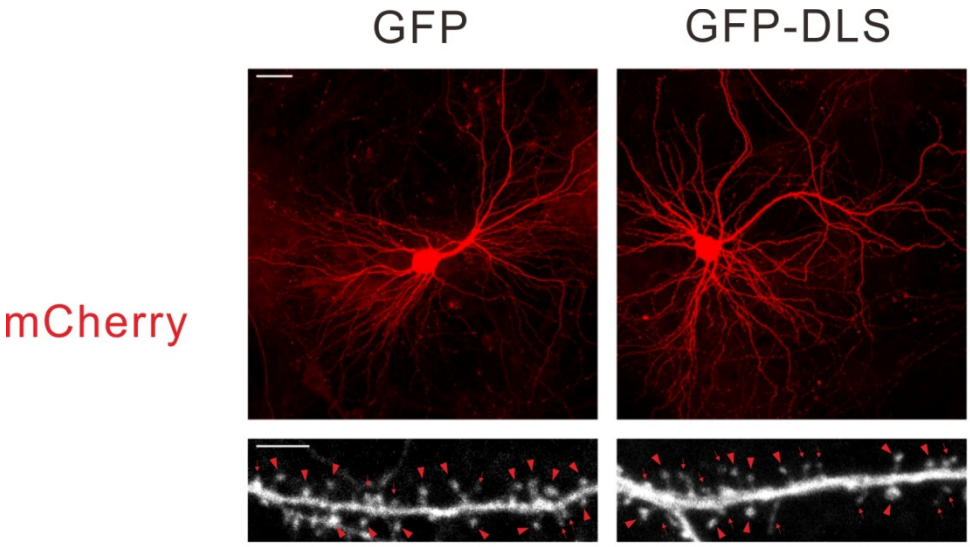

Figure S2. Overexpression of the DLS peptide leads to defects in dendritic spine development. Related to Fig. 5.

Representative images of transfected hippocampal neurons at DIV17. Arrowheads indicate mature spines with a mushroom-like head, and arrows represent immature spine types including filopodia, branchy, stubby and thin mushrooms. Scale bars indicate 30 μm (higher panel) and 3 μm (lower panel), respectively.

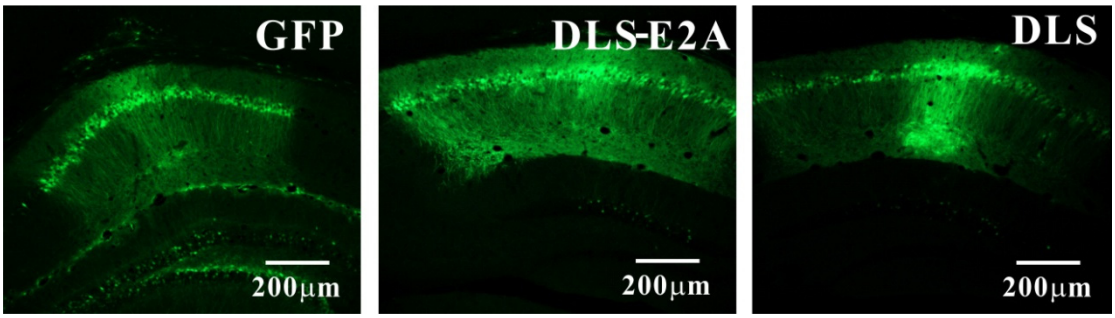

Figure S3. Representative images (top) showing the expression of GFP, GFP-DLS-E2A and GFP-DLS peptides in the CA1 region of adult mouse hippocampus 7 days after the injection of LV-Ubi-MCS-eGFP, LV-Ubi-MCS-DLS-E2A-eGFP or LV-Ubi-MCS-DLS-eGFP virus particles. Related to Fig. 5.

Supplemental Tables

Table S1. Data collection and refinement statistics (Related to Figures 1 and 5)

	PSD-95 GK/pSAPAP1-R2	PSD-95 SH3-GK/GKI-QSF
Data collection		
Source	SSRF-BL17U	SSRF-BL19U
Wavelength (Å)	0.97915	0.97853
Space group	P212121	C2
Cell dimensions		
a, *b*, *c* (Å)	33.776, 84.063, 165.123	119.028, 45.743, 86.358
Resolution (Å)	50.00–2.30 (2.34 -2.30)	50.00–2.35 (2.39 -2.35)
R_{merge}[a] (%)	12.6 (50.4)	6.8 (69.4)
Redundancy	6.5 (6.7)	5.8 (6.0)
$I / \sigma I$	17.1 (4.4)	16.3 (1.8)
Completeness (%)	99.1 (99.9)	99.2 (99.4)
Refinement		
Resolution (Å)	36.46-2.30 (2.37-2.30)	36.74-2.35 (2.43-2.35)
R_{work}[b]/R_{free}[c] (%)	16.94 (18.46)/22.27 (26.64)	19.82 (26.01)/25.00 (27.62)
No. of reflections		
Working set	21663 (1909)	18960 (1862)
Test set	1116 (98)	974 (95)
Rmsd bonds (Å)/angles (°)	0.028/1.04	0.010/0.99
No. atoms		
Protein	3140	2262
Solvent	225	45
B-factors		
Protein	32.81	73.9
Peptide	37.13	99.6
Ramachandran Plot (%)		
Favored region	98	94.5
Allowed region	2.1	4.4
Generously allowed	0	1.1

Values in parentheses are for highest-resolution shell.

a. $R_{merge} = \sum|I_i - I_m|/\sum I_i$, where I_i is the intensity of the measured reflection and I_m is the mean intensity of all symmetry related reflections.

b. $R_{work} = \Sigma||F_{obs}| - |F_{calc}||/\Sigma|F_{obs}|$, where F_{obs} and F_{calc} are observed and calculated structure factors in the refinement.

c. $R_{free} = \Sigma_T||F_{obs}| - |F_{calc}||/\Sigma_T|F_{obs}|$, where T is a test data set of about 5% of the total reflections randomly chosen and set aside prior to refinement.

Table S2. Summary of parameters of ITC assays in this study
(Related to Figures 2, 5 and 6)

Interactions	N	Kd[μM]	ΔH [cal/mol]	ΔS [cal/mol/deg]
pSAPAP1-R2/GK	0.713±0.002	0.08±0.01	-1.341E4±71.3	-12.5
pSAPAP3-R1/GK	0.768±0.004	0.07±0.01	-1.445E4±141.6	-15.7
pSAPAP1-R2 (R-3A)/GK	0.664±0.007	0.29±0.05	-9599±143.8	-2.29
pSAPAP1-R2/GK T611A	0.700±0.012	1.03±0.15	-1.106E4±262.2	-9.71
pSAPAP1-R2/GK T611I	0.741±0.008	1.02±0.10	-5088±78.14	10.3
pSAPAP1-R2/GK E600A	0.589±0.005	0.74±0.05	-1.346E4±150.4	-17.1
QSF/GK	0.888±0.012	1.14±0.14	-1.007E4±200.7	-6.6
MKL/GK	0.855±0.014	1.86±0.31	-1.184E4±291.4	-13.5
DLS/GK	0.891±0.009	0.66±0.13	-1.137E4±189.5	-9.87
pDLS/GK	0.695±0.002	0.004±0.000	-1.876E4±109.1	-24.8
QSF/GK A601D	0.669±0.020	4.46±0.49	-1.419E4±584.3	-23.1